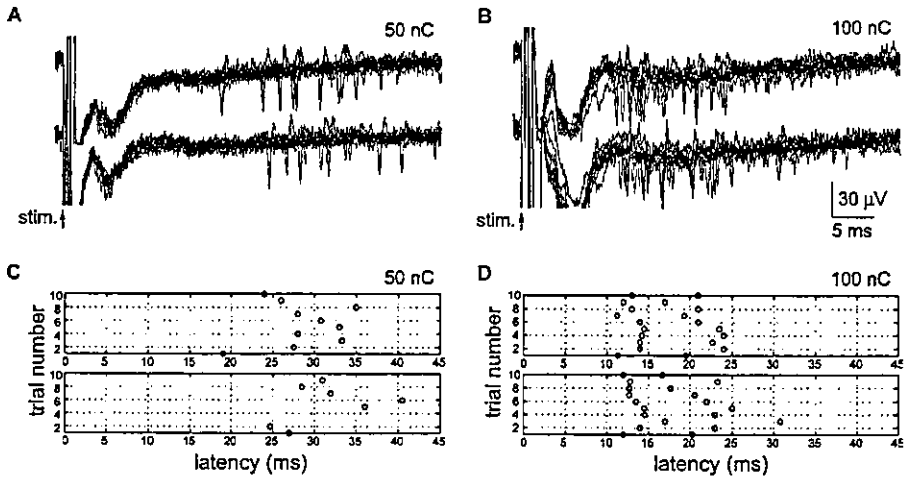

Fig. 7. Responses of a ganglion cell to stimuli with the same charge per phase but different parameters. The stimulus inter-pulse duration was 100 μs. The distance between the stimulation and the recording sites was 808 μm. Each trace is the superposition of recordings of 10 trials. (A) Responses of the ganglion cell elicited by the same charge per phase (50 nC). Upper trace: pulse amplitude, 100 μA; pulse duration, 500 μs. Lower trace: pulse amplitude, 200 μA; pulse duration, 250 μs. (B) Responses of the ganglion cell elicited by the same charge per phase (100 nC). Upper trace: pulse amplitude, 200 μA; pulse duration, 500 μs. Lower trace: pulse amplitude, 100 μA; pulse duration, 1000 μs. The arrows in (A) and (B) stand for the onset of the current stimulus. (C) and (D) is raster plots of the spikes shown in (A) and (B), respectively.

and the second one of the upper trace of B was 13.1 ± 1.2 ms (10 trials) and 21.3 ± 2.3 ms (10 trials), respectively. The latency of the first spike and the second one of the lower trace of B was 13.6 ± 1.5 ms (10 trials) and 22.2 ± 4.0 ms (10 trials), respectively. The latency including both the first and the second spikes in the upper trace and in the lower trace of B was 17.2 ± 4.6 ms (20 spikes in 10 trials) and 17.9 ± 5.3 ms (20 spikes in 10 trials), respectively.

We have made the analysis of variance (ANOVA) on these latencies (multiple comparisons, Matlab). There was no significant difference in the distribution of the latency between the upper case and the lower case in A ($P < 0.001$). There was no significant difference between the first spike of the upper case and that of the lower case in B ($P < 0.001$). There was also no significant difference between the second spike of the upper case and that of the lower case in B ($P < 0.001$). However, the upper case in A was significantly different from the upper case in B as well as from the lower case in B ($P < 0.001$). The lower case in A was also significantly different from the upper case in B as well as the lower case in B ($P < 0.001$). These results indicate that it is the charge per phase of the stimulus that defines the spike latency, and not the individual parameters of the stimuli in the range observed (5–100 nC, 20 cells in 7 retinas).

4. Discussion

This study clarified temporal properties of retinal ganglion cell responses to local transretinal current stimuli. Different waveforms of spike response were observed by the differential recording configuration. As illustrated in Fig. 2, either biphasic or triphasic spikes were recorded. Spike amplitudes ranged from 10 to 100 μV. This range is similar to that obtained by the monopolar recording configuration in which the reference electrode is set in the bath (Grumet et al., 2000; Ishikane et al., 1999; Meister, Pine, & Baylor, 1994). The three different waveforms, i.e., the biphasic, the narrow biphasic and the triphasic waveforms, were recorded in the present experiments. The waveforms of the spikes recorded by the differential configuration were similar to the spike waveforms recorded by the monopolar configuration (Ishikane et al., 1999; Meister et al., 1994). In the differential recording configuration, however, responses of reversed polarity were also recorded since the response polarity changed depending on which one of the pair of recording electrodes was in the vicinity of the recorded cell.

In light-induced responses recorded in the present study, triphasic spikes as well as narrow biphasic spikes were occasionally found with a constant delay in different pairs of electrodes that were located along a pathway of the ganglion cell axon. This suggests that those spikes are conducted along the axon of the ganglion cell.

The biphasic spike was thought to be recorded near the soma of the ganglion cell in the monopolar recording configuration (Grumet et al., 2000; Ishikane et al., 1999; Meister et al., 1994). We did not obtained any biphasic spikes indicating the conduction along the axonal pathway, which agreed with this interpretation.

4.1. Temporal pattern of the response

There were fundamentally two different classes of responses elicited by the local transretinal current stimulus. In one class, the latency was rather short (1.5–4.5 ms) and constant over trials. The latency was affected little by stimulus parameters, i.e., the amplitude and the duration, once the spike was elicited. Another class of response had the latency that was relatively long and fluctuated from trial to trial. The latency was affected by the stimulus parameters. We were not able to examine if there were spikes in a short time after the stimulus onset (less than about 2 ms but it depended on a recording) because of an artifact that could not be eliminated by the differential recording configuration. It is, however, unlikely that spikes were induced in that period since the refractory period after the spike excitation would prevent the recorded spike if there were any.

In a previous study on the rabbit retina, two types of responses exhibiting similar latency properties to those found in the present study were reported (Jensen, Ziv, & Rizzo, 2002). However, long latency responses were reported as a burst of spikes. In the present study, a single spike response with a long latency was induced around the threshold and a double spike, but not a burst, was induced as the charge applied per phase of the stimulus was increased. This difference could be due to the difference in either the animal species or the electrode arrangement. Our result suggests that the temporal pattern of the spike response train can be controlled using a corresponding stimulus pulse sequence, which will be important for retinal prostheses.

In the chicken retina, Stett et al. reported spike responses which showed several different temporal patterns, i.e., single bursts, a weak delayed discharge, and early bursts followed by periods of a silence and a delayed discharge with smaller amplitude (Stett et al., 2000). This variety might reflect the differences in arrangement of stimulus electrodes and stimulus waveform from those used in the present study. Namely, the monophasic voltage pulses were applied diffusely against grounded bath in their case. If it is the case, the locally applied transretinal electrical stimuli are considered to be more advantageous to control the temporal pattern of induced responses.

It has been reported that a diffusely applied transretinal current stimulus excited neurons more distal than ganglion cells, e.g., photoreceptors, bipolar cells and/or amacrine cells, to release neurotransmitter(s) (Byzov & Trifonov, 1968; Kaneko & Saito, 1983; Kaneko & Shimazaki, 1976; Toyoda & Fujimoto, 1984; Toyoda et al., 1977). The local transretinal current used in the present study also might be able to stimulate the presynaptic cells to excite the ganglion cells. The responses with a long and fluctuating latency observed in the present study could be the ones elicited indirectly through excitation of presynaptic cells. Further studies are necessary to clarify the mechanisms of how these two types of responses are elicited.

4.2. Effects of stimulus parameters

The effects of the amplitude and the pulse duration of electrical stimulus were studied in rabbit retinas (Grumet et al., 2000; Rizzo & Wyatt, 1997), cat pyramidal tract cells (Asanuma, Arnold, & Zarzecki, 1976; Stoney, Thompson, & Asanuma, 1968) and the cat spinal cord (West & Wolstencroft, 1983). A model study has also been performed (McIntyre & Grill, 2002). These studies reveal that the threshold of the excitation decreases as the pulse duration increases up to a certain value and further increase of the duration does not affect the threshold (Asanuma et al., 1976; McIntyre & Grill, 2002; Stoney et al., 1968; West & Wolstencroft, 1983).

It has been suggested that the threshold of the stimulus can be evaluated with a total charge applied to the tissue. This was confirmed for the local transretinal current stimulus used in the present study. In this study the threshold and the latency of the response were defined by the total charge per phase of the stimulus, and not the individual parameters of the stimuli.

In this study, charge-balanced biphasic current stimuli were used to induce ganglion cell responses. Such stimuli are favorable for clinical applications since they are believed to minimize the electrical damage to neural tissue and electrodes (Bartlett et al., 1977; Brummer & Turner, 1977; Lilly et al., 1955; Margalit et al., 2002; Tehovnik, 1996). The interval of the two phases of the biphasic stimulus affected the threshold of ganglion cell excitation. The stimulus with a longer inter-pulse duration had a lower threshold to excite the ganglion cell than that with a shorter inter-pulse duration (Figs. 3C and 6). Once the spike was induced, however, a further increase of the inter-pulse duration did not affect the spike properties. This means that the second negative pulse had a suppressive effect on the first positive pulse. The inter-pulse duration at which the second pulse lost the suppressive effect on the first pulse was different in different ganglion cells and was dependent on the charge applied.

Acknowledgments

The authors thank Dr. A.T. Ishida for comments on the manuscript. This work was supported by the Japan Society for the Promotion of Science, grant-in-aid for Research for the Future Program, JSPS-RFTF 97I00101 (PI: Prof. T. Yamakawa).

References

Asanuma, H., Arnold, A., & Zarzecki, P. (1976). Further study on the excitation of pyramidal tract cells by intracortical microstimulation. *Experimental Brain Research, 26*, 443–461.

Bartlett, J. R., Doty, R. W., Lee, B. B., Negrao, N., & Overman, W. H. (1977). Deleterious effects of prolonged electrical excitation of striate cortex in macaques. *Brain, Behavior and Evolution, 14*, 46–66.

Brummer, S. B., & Turner, M. J. (1977). Electrochemical considerations for safe electrical stimulation of the nervous system with platinum electrodes. *IEEE Transactions on Biomedical Engineering, 24*, 59–63.

Byzov, A. L., & Trifonov, Ju. A. (1968). The response to electric stimulation of horizontal cells in the carp retina. *Vision Research, 8*, 817–822.

Chow, A. Y., & Chow, V. Y. (1997). Subretinal electrical stimulation of the rabbit retina. *Neuroscience Letters, 225*, 13–16.

Eckmiller, R. (1997). Learning retina implants with epiretinal contacts. *Ophthalmic Research, 29*, 281–289.

Greenberg, R. J., Velte, T. J., Humayun, M. S., Scarlatis, G. N., & de Juan, E. Jr., (1999). A computational model of electrical stimulation of the retinal ganglion cell. *IEEE Transactions on Biomedical Engineering, 46*, 505–514.

Grumet, A. E., Wyatt, J. L., & Rizzo, J. F. (2000). Multi-electrode stimulation and recording in the isolated retina. *Journal of Neuroscience Methods, 101*, 31–42.

Hesse, L., Schanze, T., Wilms, M., & Eger, M. (2000). Implantation of retina stimulation electrodes and recording of electrical stimulation responses in the visual cortex of the cat. *Graefe's archive for clinical and experimental ophthalmology, 238*, 840–845.

Humayun, M., Propst, R., de Juan, E., Jr., McCormick, K., & Hickingbotham, D. (1994). Bipolar surface electrical stimulation of the vertebrate retina. *Archives of Ophthalmology, 112*, 110–116.

Humayun, M., Sato, Y., Propst, R., & de Juan, E. Jr., (1995). Can potentials from the visual cortex be elicited electrically despite severe retinal degeneration and a markedly reduced electroretinogram?. *German Journal of Ophthalmology, 4*, 57–64.

Humayun, M. S. (2001). Intraocular retinal prosthesis. *Transactions of the American Ophthalmological Society, 99*, 271–300.

Humayun, M. S., de Juan, E., Jr., Dagnelie, G., Greenberg, R. J., Propst, R. H., & Phillips, D. H. (1996). Visual perception elicited by electrical stimulation of retina in blind humans. *Archives of Ophthalmology, 114*, 40–46.

Humayun, M. S., de Juan, E., Jr., Weiland, J. D., Dagnelie, G., Katona, S., Greenberg, R., et al. (1999). Pattern ele ctrical stimulation of the human retina. *Vision Research, 39*, 2569–2576.

Ishikane, H., Kawana, A., & Tachibana, M. (1999). Short- and long-range synchronous activities in dimming detectors of the frog retina. *Visual Neuroscience, 16*, 1001–1014.

Jensen, R. J., Ziv, O. R., & Rizzo, J. F. (2002). Effect of epiretinal vs transretinal in vitro electrical stimulation of rabbit retinal ganglion cells. *Investigative Ophthalmology and Visual Science, 43*, 4473 (E-Abstract).

Kaneko, A., & Saito, T. (1983). Ionic mechanisms underlying the responses of off-center bipolar cells in the carp retina. Studies on responses evoked by transretinal current stimulation. *The Journal of General Physiology, 81*, 603–612.

Kaneko, A., & Shimazaki, H. (1976). Synaptic transmission from photoreceptors to bipolar and horizontal cells in the carp retina. *Cold Spring Harbor Symposia on Quantitative Biology, 40*, 537–546.

Li, L., Kameda, K., Hayashida, Y., & Yagi, T. (2001). On a retinal prosthesis using a silicon retina. *Annals of Biomedical Engineering, 29*(Suppl. 1), S-2 (Abstract).

Lilly, J. C., Hughes, J. R., Alvord, E. C., & Galkin, T. W. (1955). Brief, noninjurious electric waveform for stimulation of the brain. *Science, 121*, 468–469.

Margalit, E., Maia, M., Weiland, J. D., Greenberg, R. J., Fujii, G. Y., Torres, G., et al. (2002). Retinal prosthesis for the blind. *Survey of Ophthalmology, 47*, 335–356.

McIntyre, C. C., & Grill, W. M. (2002). Extracellular stimulation of central neurons: Influence of stimulus waveform and frequency on neuronal output. *Journal of Neurophysiology, 88*, 1592–1604.

Meister, M., Pine, J., & Baylor, D. A. (1994). Multi-neuronal signals from the retina: Acquisition and analysis. *Journal of Neuroscience Methods, 51*, 95–106.

Murakami, M., & Takahashi, K. (1987). Calcium action potential and its use for measurement of reversal potentials of horizontal cell responses in carp retina. *The Journal of Physiology, 386*, 165–180.

Oka, H., Shimono, K., Ogawa, R., Sugihara, H., & Taketani, M. (1999). A new planar multielectrode array for extracellular recording: Application to hippocampal acute slice. *Journal of Neuroscience Methods, 93*, 61–67.

Peyman, G., Chow, A. Y., Liang, C., Chow, V. Y., Perlman, J. I., & Peachey, N. S. (1998). Subretinal semiconductor microphotodiode array. *Ophthalmic Surgery and Lasers, 29*, 234–241.

Ranck, J. B. (1975). Which elements are excited in electrical stimulation of mammalian central nervous system: A review. *Brain Research, 98*, 417–440.

Rizzo, J. F., & Wyatt, J. (1997). Prospects for a visual prosthesis. *The Neuroscientist, 3*, 251–262.

Stett, A., Barth, W., Weiss, S., Haemmerle, H., & Zrenner, E. (2000). Electrical multisite stimulation of the isolated chicken retina. *Vision Research, 40*, 1785–1795.

Stoney, S. D., Thompson, W. D., & Asanuma, H. (1968). Excitation of pyramidal tract cells by intracortical microstimulation: Effective extent of stimulating current. *Journal of Neurophysiology, 31*, 659–669.

Takahashi, K., & Murakami, M. (1988). Calcium action potential in ON-OFF transient amacrine cell of the carp retina. *Brain Research, 456*, 29–37.

Tehovnik, E. J. (1996). Electrical stimulation of neural tissue to evoke behavioral responses. *Journal of Neuroscience Methods, 65*, 1–17.

Toyoda, J., & Fujimoto, M. (1984). Application of transretinal current stimulation for the study of bipolar-amacrine transmission. *The Journal of General Physiology, 84*, 915–925.

Toyoda, J., Fujimoto, M., & Saito, T. (1977). Responses of second-order neurons to photic and electric stimulation of the retina. In H. B. Barlow & P. Fatt (Eds.), *Vertebrate Photoreception* (pp. 231–250). London, New York, San Francisco: Academic Press Inc.

Trifonov, Yu. A. (1968). Study of synaptic transmission between the photoreceptor and the horizontal cell using electrical stimulation of the retina. *Biofizika, 13*, 809–817.

Walter, P., & Heimann, K. (2000). Evoked cortical potentials after electrical stimulation of the inner retina in rabbits. *Graefe's Archive for Clinical and Experimental Ophthalmology, 238*, 315–318.

Weiland, J. D., Humayun, M. S., Dagnelie, G., de Juan, E., Jr., Greenberg, R. J., & Iliff, N. T. (1999). Understanding the origin of visual percepts elicited by electrical stimulation of the human retina. *Graefe's Archive for Clinical and Experimental Ophthalmology, 237*, 1007–1013.

West, D. C., & Wolstencroft, J. H. (1983). Strength-duration characteristics of myelinated and non-myelinated bulbospinal axons in the cat spinal cord. *The Journal of Physiology, 337*, 37–50.

Wyatt, J., & Rizzo, J. (1996). Ocular implants for the blind. *IEEE Spectrum, 33*, 47–53.

Zrenner, E. (2002). Will retinal implants restore vision?. *Science, 295*, 1022–1025.

Zrenner, E., Miliczek, K. D., Gabel, V. P., Graf, H. G., Guenther, E., Haemmerle, H., et al. (1997). The development of subretinal microphotodiodes for replacement of degenerated photoreceptors. *Ophthalmic Research, 29*, 269–280.

Zrenner, E., Stett, A., Weiss, S., Aramant, R. B., Guenther, E., Kohler, K., et al. (1999). Can subretinal microphotodiodes successfully replace degenerated photoreceptors?. *Vision Research, 39*, 2555–2567.

Jpn J Ophthalmol 2004;48:256–261
© Japanese Ophthalmological Society 2004

DOI 10.1007/s10384-004-0055-1

LABORATORY INVESTIGATION

Transretinal Electrical Stimulation with a Suprachoroidal Multichannel Electrode in Rabbit Eyes

Hirokazu Sakaguchi[1], Takashi Fujikado[1], Xiaoyun Fang[1], Hiroyuki Kanda[1], Makoto Osanai[2], Kazuaki Nakauchi[1], Yasushi Ikuno[1], Motohiro Kamei[1], Tohru Yagi[3], Shigeru Nishimura[3], Masahito Ohji[1], Tetsuya Yagi[2], and Yasuo Tano[1]

[1]Department of Ophthalmology, Graduate School of Medicine, Osaka University, Suita, Japan; [2]Department of Electronic Engineering, Graduate School of Engineering, Osaka University, Suita, Japan; [3]Nidek Co., Ltd., Gamagori, Japan

Abstract

Purpose: Several approaches for placing an electrode device for visual prosthesis have been previously proposed. In this study, we investigated if transretinal stimulation from the suprachoroidal space can elicit an electrical evoked potential (EEP) in albino rabbits.

Methods: A flat electrode array (polyimide plate, platinum electrode) was developed and used for this study. After performing a scleral incision at 2–2.5 mm from the limbus and placing an anchoring suture, the array was inserted into the suprachoroidal space in the posterior portion of the eye by direct observation under a microscope. A platinum wire was implanted into the vitreous space as a reference electrode. For electrical stimulation, a biphasic pulse was used. When the electrode was stimulated, the EEP was recorded.

Results: When the electrical stimulation from the suprachoroidal space was applied, the EEP could be recorded with an epidural electrode, and the threshold was 66.0 ± 32.1 μA (42.0 μC/cm^2). Histological examination indicated the absence of major damage to the retina and choroid from the insertion and placement of the array and the electrical stimulation.

Conclusions: Transretinal electrical stimulation from the suprachoroidal space could elicit EEP, suggesting that this approach may be useful for a retinal prosthesis system. **Jpn J Ophthalmol** 2004;48:256–261
© Japanese Ophthalmological Society 2004

Key Words: electrical stimulation, electrode, suprachoroid, transretinal stimulation, visual prosthesis

Introduction

In 1974, Dobelle et al.[1] demonstrated that a totally blind patient could sense light with stimulation from an electrode in the visual cortex. Since this presentation, the possibility of artificial vision has been recognized, and many groups have tried to develop a visual prosthesis for blind patients.[2–18]

Several methods for the placement of an electrode that can stimulate visual neurons were developed. Dobelle et al. developed the method of stimulating the surface of the visual cortex.[1,3–5] Several other groups have tried to stimulate the retina with different types of electrodes; some groups have developed subretinal electrodes,[6–10] and other groups have developed epiretinal electrodes.[11–18]

There is a rationale for electrically stimulating the retinal neuronal cells with an electrode for visual prosthe-

Received: January 15, 2004 / Accepted: February 2, 2004
Correspondence and reprint requests to: Hirokazu Sakaguchi, Department of Ophthalmology, Graduate School of Medicine, Osaka University, E-7, 2-2 Yamadaoka, Suita 565-0871, Japan
e-mail: sakaguh@ophthal.med.osaka-u.ac.jp

sis. According to Santos et al.,[15] in the retinas of patients suffering from advanced retinitis pigmentosa, 78% of the bipolar cells and 30% of the ganglion cells remain intact.

In this study, we developed a flat electrode array and a method for inserting the array into the suprachoroidal space. We also determined if the transretinal stimulation from this space could elicit an electrical evoked potential (EEP) in albino rabbits.

Materials and Methods

Animals

Five eyes from five Japanese white rabbits, obtained from Hokusetsu (Setsu, Osaka, Japan) and each weighing 2.0 to 2.5 kg, were used in this study. All experiments were performed in accordance with the Association for Research in Vision and Ophthalmology Statement for the Use of Animals in Ophthalmic and Vision Research and the policies in the Guide to the Care and Use of Laboratory Animals issued by the National Institutes of Health, USA.

To anesthetize each rabbit, an intramuscular injection of ketamine hydrochloride (32 mg/kg body weight) and xylazine hydrochloride (4 mg/kg body weight) were used.

Setting of Cortex Electrode

While the animal was under anesthesia, the top of the skull was exposed and drilled at a point on the forehead 8 mm from the sutura lambdoidea and 7 mm right and left of the meridian. Then, screw-type stainless electrodes, coated with silver, were screwed into the skull and attached to the dura mater.[19]

Bright-flash Visual Evoked Potential

A bright-flash visual evoked potential (VEP) was elicited before transretinal electrical stimulation to compare its implicit time and waveform with those of the EEP. While the animals were under anesthesia, the eyes were dilated with topical 0.5% phenylephrine hydrochloride and 0.5% tropicamide.

The VEP was evaluated from the screw-type electrode opposite the stimulated eye. VEP was performed with white flashes. The light stimulus was regulated by a stimulator (SLS-3100, Nihon Kohden, Tokyo, Japan), and the flash device (LS-704B, Nihon Kohden) was placed 15 cm above the eye level of the animal to make the basic line of the VEP linear. The VEP waveforms were recorded and calculated by a computer (Neuropack 2, MEB-7202, Nihon Kohden). The energy of the flash was constant at 1.2 J. The results from 50 trials for each eye were averaged and analyzed.

A Flat Electrode Array

A flat electrode array was developed (Fig. 1). The array body was made of polyimide epoxy resin. The length, thickness, and width of the top of the array were 130 mm, 50 μm, and 2 mm, respectively. Eight round electrodes made of gold were within the array body, not mounted on the body, so that damage to the tissues would be minimal when inserting the array into the suprachoroidal space. The electrodes were connected by copper lines in the array body. The distance between electrodes was 500 μm.

The impedance of each electrode was examined. The frequency dependency of the impedance is shown in Fig. 2. A 100-mV (peak-to-peak) signal, 500 Hz to 100 kHz AC, was applied to the electrodes during this measurement.

Insertion of the Electrode into Suprachoroidal Space

The pupils were dilated with 0.5% phenylephrine hydrochloride and 0.5% tropicamide. Under a surgical microscope (OPMI 6-S, Zeiss, Oberkochen, Germany), a 2-mm scleral incision was made 2–2.5 mm posterior to the limbus and the choroid was exposed (Fig. 3A). The electrode array was inserted into the entrance of the space between the sclera and choroid through the anchoring suture (Fig. 3B). With a contact lens on the cornea, the electrode array was inserted gradually until the top of the array was in the posterior portion of the eye (Fig. 3C).

Electrical Stimulation and Measurement of EEP at the Visual Cortex

A biphasic pulse was used for the electrical stimulation. The biphasic pulse consisted of one current (suprachoroid to vitreous) and a second opposing current (vitreous to suprachoroid). Both currents had a duration of 0.5 ms. A biphasic pulse with opposite polarization was also used to examine if the direction of the current affected the EEP. The current was varied as follows: 500, 200, 100, 50, 30, 20, and 10 μA. The current was produced with an electronic stimulator (SEN-7203, Nihon Kohden) and a linear isolator (World Precision Instruments, Sarasota, FL, USA). A platinum wire was implanted into the vitreous space as a reference electrode. With the transretinal stimulation, EEP was investigated with the epidural electrode opposite to the stimulated eye; the EEP waveforms were recorded and calculated by a computer (Neuropack 2). The results from 50 trials for each eye were averaged and analyzed. The threshold and implicit time of the first positive wave were evaluated. The implicit time at a stimulation of 50 μA was compared with that of the VEP's first positive wave by student's paired t test. Statistical significance was assumed when P was <0.05; all tests were two-tailed. To make sure the potential originated from the transretinal electrical stimulation within the suprachoroidal space, the same procedures were also performed after removal of the optic nerve underneath the eyeball.

Jpn J Ophthalmol
Vol 48: 256–261, 2004

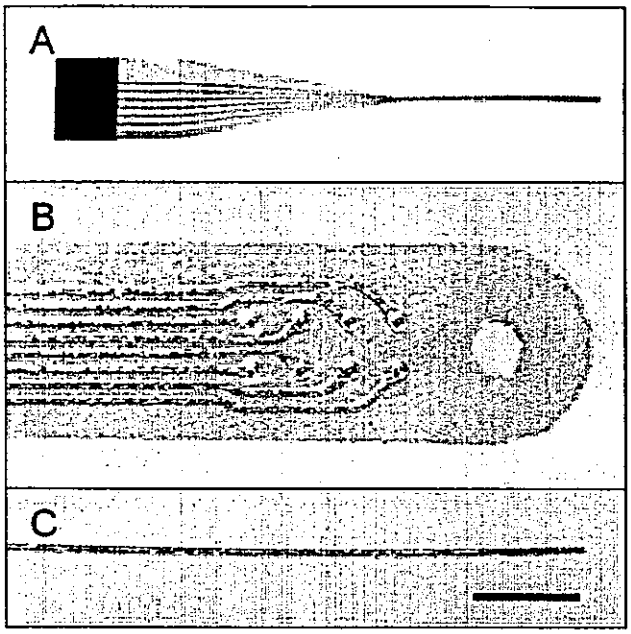

Figure 1A–C. The flat electrode array. **A** The array body is made of polyimide. Its length is 130 mm and the width at its top is 2 mm. **B** High magnification of the top of the array. The electrodes are made of platinum and attached by copper lines in the array body. The diameter of the round electrode is 100 μm, and the distance between electrodes is 500 μm. **C** High magnification of the top of the array. The thickness of the array is 50 μm. The electrodes do not protrude from the array body, and the array is flat. Bar = 1 mm for **B** and **C**.

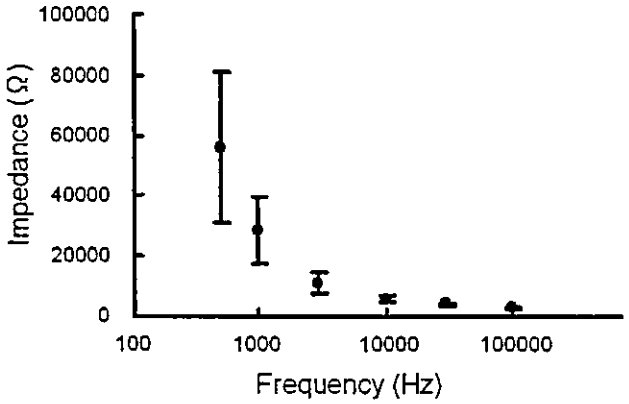

Figure 2. The impedance of the electrodes. Frequency dependency of the impedance is shown. Values are average ± SD, $n = 3$. A 100-mV (peak-to-peak) signal, 500 Hz to 100 kHz AC, was applied to the electrodes during this measurement.

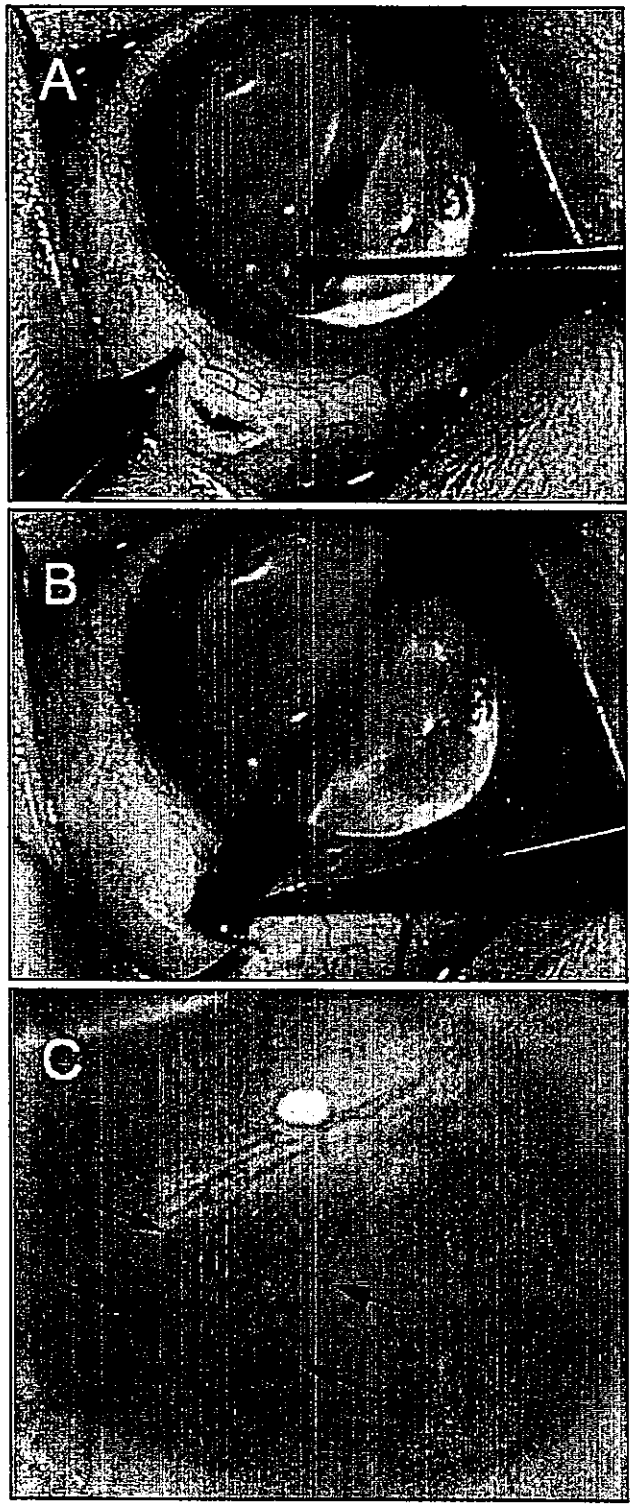

Figure 3A–C. The insertion of a flat electrode into the suprachoroidal space. **A** A scleral incision is made at 2–2.5 mm from the limbus. The choroid is exposed, and the anchoring suture is made. The top of the array is grasped by forceps. **B** The top of the array is inserted into the suprachoroidal space. **C** Under a surgical microscope, the electrode array can be seen clearly under the retina and choroid vessels (*arrows*). Because the array is flat, the damage to the choroidal vessels is minimal, and there are no major complications around the top of the array.

Histological Study

To examine the complications to the retina or choroid from the transretinal electrical stimulation, or from the insertion and placement of the array itself, a histological study was performed on tissues adjacent to the areas where the electrode was placed. After examination of the EEP with electrical stimulation, the array was removed from the eyes and the rabbits were killed with a 5-ml intravenous injection of pentobarbital (50mg/ml). The eyes were enucleated, dissected, and embedded in paraffin after incubation in 4% paraformaldehyde. Three-micrometer-thick paraffin sections were stained with H&E. The sections were examined by light microscopy, and the images were digitized using a CCD camera (AxioCam, Carl Zeiss Japan, Tokyo, Japan) and processed with AxioVision 2.0 (Carl Zeiss Japan) software on a Windows computer.

Results

The Electrode Array Under the Retina and Choroid

With a surgical microscope, the electrode array could be clearly seen under the retinal and choroidal vessels in the posterior portion of the eye. There were no major complications, such as retinal detachment, around the top of the array at the posterior portion (Fig. 3C).

The EEP with Varied Transretinal Electrical Stimulation

The EEP from all five eyes could be recorded with transretinal electrical stimulation. An example of an EEP with two types of biphasic current from an eye is shown in Fig. 4. The waves on the right were obtained with the biphasic pulse consisting of one current (suprachoroid to vitreous) and a second opposing current (vitreous to suprachoroid). Those on the left were obtained when the pulse consisted of opposite components. The smallest threshold from each of the five eyes was 66.0 ± 32.1 μA and 94.0 ± 68.4 μA (average ± SD) for each current direction, respect ($n = 5$) There was no statistical difference between different polarities ($P > 0.05$). With the superficial dimension, the averaged electrical density was 42.0 μC/cm² and 59.8 μC/cm², respectively. The implicit times of the first positive waves of the EEP with the two types of biphasic current were 9.0 ± 1.0 and 8.7 ± 0.9 ms, respectively (Fig. 4), and there was no statistical difference between polarities.

The Comparison Between Bright-flash VEP and the EEP

Bright-flash VEP waves were obtained from all five eyes, and the implicit time of the first positive wave was 21.7 ± 0.6 ms (average ± SD; Fig. 5, top). They were statistically longer than those of the EEP (Fig. 5, bottom, $P < 0.001$). The waveform of the EEP resembled the VEP waveform.

After cutting the optic nerve behind the eyes, the wave was not different from the baseline (data not shown).

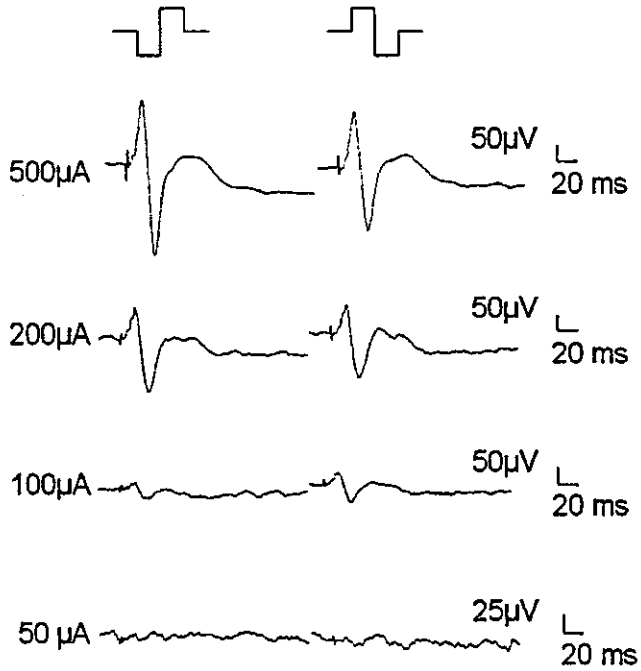

Figure 4. The electrical evoked potential (EEP) from a rabbit eye by transretinal electrical stimulation. *Left*: EEP waves obtained with a biphasic current consisting of suprachoroid to vitreous transretinal electrical stimulation and vitreous to suprachoroid stimulation. *Right*: EEP waves with currents with opposite polarization.

Histological Study

Histological examination of the sections around the suprachoroidal space into which the flat electrode array had been inserted demonstrated no severe complications such as retinal detachment after the insertion of the array and after a series of electrical stimulations (Fig. 6A).

Discussion

In this study, we developed a flat electrode array and were able to safely insert the array into the suprachoroidal space of albino rabbits. We performed the insertion into this space in the posterior portion of the eyes through a scleral incision at the limbus. We also showed that transretinal electrical stimulation from the suprachoroidal space could elicit an EEP.

Several methods can be used to stimulate the visual neurons for visual prosthesis: stimulation at the visual cortex, and stimulation of retinal neurons from a subretinal

Jpn J Ophthalmol
Vol 48: 256–261, 2004

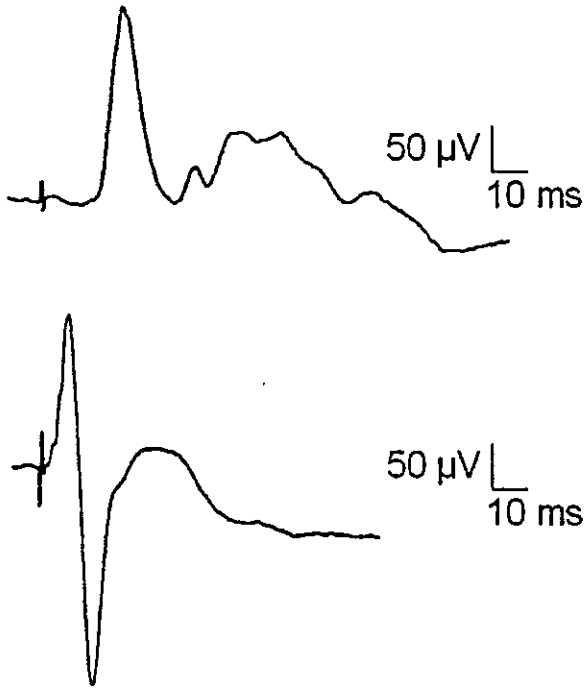

Figure 5. Comparison of waveforms between bright-flash visual evoked potential (VEP) and the electric evoked potential (EEP) from a rabbit eye. *Top*: A VEP wave consists of several positive waves. The implicit time of the first positive wave was 22.0 ms. *Bottom*: An EEP wave also consists of several positive waves. The implicit time of the first positive wave was 9.0 ms.

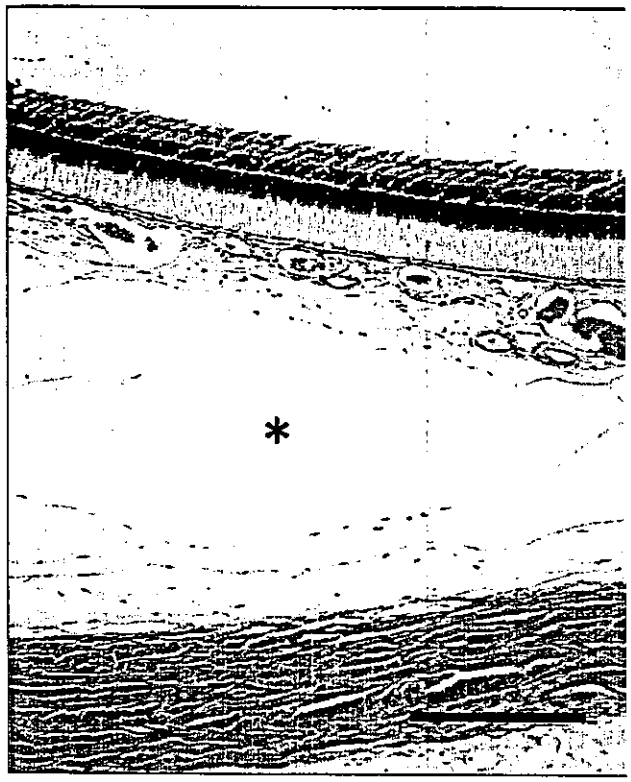

Figure 6. Results of the histological study of the suprachoroidal space where the flat electrode array was placed. The area around the space where the electrode array was placed (*) demonstrates no major complications such as retinal detachment or bleeding from the insertion of the array or after a series of electrical stimulations. Bar = 250 μm.

space or from the epiretinal side. On group also successfully developed a method for stimulation of the optic nerve in front of the chiasma.[20] All methods except stimulation of the retina require intracranial surgery, which has the risk of severe complications. Our method does not require intracranial surgery, and the insertion of the electrode into the suprachoroidal space is thought to be safer than the methods requiring intracranial surgery.

When the electrodes are placed at the epiretinal lesion or in the subretinal space, retinal detachment may occur. Because our method is not dependent upon the attachment of the array to the retina itself, it is comparatively safer.

Histological analysis in this study showed the separation of the choroidal tissues and sclera. This separation could lead to the breaking of the choroidal vessels and hemorrhage. Our short-term study showed no distinct hemorrhage around the top of the electrode array. A long-term study is required in the future to confirm this result.

The EEP waveforms by transretinal electrical stimulation resembled those of the bright-flash VEP. Implicit time of the EEP was 9.0 ± 1.0 or 8.7 ± 0.9 ms for each polarized biphasic pulse, and was statistically shorter compared with that of the flash VEP wave (21.7 ± 0.6 ms). This difference may be because of the longer time it takes for the flash of light to reach the photoreceptors and for the generated signal to travel along the nerves to the ganglion cells. The transretinal electrical current can stimulate the ganglion cells and nerve fibers directly.

It has been reported that the threshold of electrical density with an epiretinal implant is 1 to 12 μC/cm^2,[18] It has also been demonstrated that the threshold with a subretinal implant is 70 μC/cm^2,[9] According to these data, the threshold in our study is almost as low as that with a subretinal implant. With the subretinal implant, the photoreceptors or the bipolar cells are thought to be stimulated. With the epiretinal implant, the nerve fiber and ganglion cell layers may be stimulated. Although our device can stimulate each layer in the retina, including the nerve fiber and ganglion cell layers, with transretinal electrical stimulation, the choroidal tissues could cause resistance. This is a possible reason why the threshold in our study is much higher than that for an epiretinal implant. In contrast, because of the transretinal electrical stimulation, our device can be used with patients suffering from diseases involving severe damage to the photoreceptor layer, such as retinitis pigmentosa.

We demonstrated the possibility of using this flat electrode array for a visual prosthesis. To utilize this device in blind people, safety precautions for long-term electrode

placement in the eyes are required. We believe that this flat suprachoroidal electrode is a significant step toward realizing our goal of providing a prosthesis that will definitely benefit blind patients.

Acknowledgment. This work was supported by a Health Sciences Research Grant, Ministry of Health, Labor, and Welfare, Japan.

References

1. Dobelle WH, Mladejovsky MG. Phosphenes produced by electrical stimulation of human occipital cortex, and their application to the development of a prosthesis for the blind. J Physiol 1974;243:553–576.
2. Zrenner E. Will retinal implants restore vision? Science 2002;295:1022–1025.
3. Dobelle WH. Artificial vision for the blind by connecting a television camera to the visual cortex. ASAIO J 2000;46:3–9.
4. Normann RA, Warren DJ, Ammermuller J, Fernandez E, Guillory S. High-resolution spatio-temporal mapping of visual pathways using multi-electrode arrays. Vision Res 2001;41:1261–1275.
5. Schmidt EM, Bak MJ, Hambrecht FT, Kufta CV, O'Rourke DK, Vallabhanath P. Feasibility of a visual prosthesis for the blind based on intracortical micfostimulation of the visual cortex. Brain 1996;119:507–522.
6. Chow AY, Chow VY. Subretinal electrical stimulation of the rabbit retina. Neurosci Lett 1997;225:13–16.
7. Peachey NS, Chow AY. Subretinal implantation of semiconductor-based photodiodes: progress and challenges. J Rehabil Res Dev 1999;36:371–376.
8. Peyman G, Chow AY, Liang C, Chow VY, Perlman JI, Peachey NS. Subretinal semiconductor microphotodiode array. Ophthalmic Surg Lasers 1998;29:234–241.
9. Schwahn HN, Gekeler F, Kohler K, et al. Studies on the feasibility of a subretinal visual prosthesis: data from Yucatan micropig and rabbit. Graefes Arch Clin Exp Ophthalmol 2001;239:961–967.
10. Zrenner E, Miliczek KD, Gabel VP, et al. The development of subretinal microphotodiodes for replacement of degenerated photoreceptors. Ophthalmic Res 1997;29:269–280.
11. Eckmiller R. Learning retina implants with epiretinal contacts. Ophthalmic Res 1997;29:281–289.
12. Walter P, Szurman P, Vobig M, et al. Successful long-term implantation of electrically inactive epiretinal microelectrode arrays in rabbits. Retina 1999;19:546–552.
13. Humayun MS, de Juan E Jr, Dagnelie G, Greenberg RJ, Propst RH, Phillips DH. Visual perception elicited by electrical stimulation of retina in blind humans. Arch Ophthalmol 1996;114:40–46.
14. Humayun MS, de Juan E Jr, Weiland JD, et al. Pattern electrical stimulation of the human retina. Vision Res 1999;39:2569–2576.
15. Santos A, Humayun MS, de Juan E Jr, et al. Preservation of the inner retina in retinitis pigmentosa. A morphometric analysis. Arch Ophthalmol 1997;115:511–515.
16. Grumet AE, Wyatt JL Jr, Rizzo JF 3rd. Multi-electrode stimulation and recording in the isolated retina. J Neurosci Methods 2000;101:31–42.
17. Rizzo JF 3rd, Wyatt J, Humayun M, et al. Retinal prosthesis: an encouraging first decade with major challenges ahead. Ophthalmology 2001;108:13–14.
18. Walter P, Heimann K. Evoked cortical potentials after electrical stimulation of the inner retina in rabbits. Graefes Arch Clin Exp Ophthalmol 2000;238:315–318.
19. Yanagida K, Miyake Y. Electrically Evoked Response (EER) in the rabbit. Nippon Ganka Gakkai Zasshi (Acta Soc Ophthalmol Jpn) 1984;88:997–1006.
20. Veraart C, Raftopoulos C, Mortimer JT, et al. Visual sensations produced by optic nerve stimulation using an implanted self-sizing spiral cuff electrode. Brain Res 1998;813:181–186.

Luminance Dependence of Neural Components that Underlies the Primate Photopic Electroretinogram

Shinji Ueno, Mineo Kondo, Yasuhiro Niwa, Hiroko Terasaki, and Yozo Miyake

PURPOSE. At lower stimulus intensities, the amplitude of the photopic flash ERG b-wave increases with increasing stimulus intensities, but then plateaus and decreases at higher stimulus intensities (the "photopic hill"). The purpose of this study was to determine the mechanism underlying this unusual phenomenon.

METHODS. Five adult monkeys (*Macaca mulatta* and *M. fascicularis*) were studied. Stimuli were obtained from xenon strobe flashes, and the intensity was reduced by neutral-density filters in 0.4-log unit steps. *N*-methyl-D-aspartic acid and tetrodotoxin citrate (NMDA+TTX) were used to suppress inner retinal activities and L-2 amino-4-phosphonobutyric acid (APB) and *cis*-2,3 piperidine dicarboxylic acid (PDA) to block postreceptoral ON- and OFF-pathway activities. The postsynaptic ON- and OFF-components were isolated by subtracting the postdrug ERGs from the predrug ERGs.

RESULTS. The intensity–response curve of the photopic b-wave obtained after the intravitreal injection of TTX+NMDA had the same shape as a photopic hill, suggesting that the contribution from the inner retinal neurons to the photopic hill is not significant. At low and intermediate intensities, the photopic b-wave was mainly shaped by the overlapping of two positive peaks from the ON- and OFF-components. However, the amplitude of the positive peak from the ON-component became smaller and broader at higher stimulus intensities. In addition, the timing of the positive peak of the OFF-component was gradually delayed with increasing intensities. After APB+PDA, the remaining cone photoreceptor component contributed only to the negative a-wave at all stimulus intensities.

CONCLUSIONS. The photopic hill in the primate ERG results mainly from two factors: the reduction of the ON-component amplitude at higher intensities and the delay in the positive peak of the OFF-component at higher intensities. (*Invest Ophthalmol Vis Sci.* 2004;45:1033–1040) DOI:10.1167/iovs.03-0657

Photopic electroretinograms (ERGs) are generated by different types of retinal cells[1–10] and are used to assess the functioning of the cone system in normal subjects and patients with various types of retinal diseases. The intensity–response function of the photopic flash ERG b-wave is not a simple function, because at lower and intermediate stimulus intensities, the amplitude of the photopic ERG b-wave increases as the intensity is increased as expected, but at still higher stimulus intensities, the amplitude unexpectedly decreases. This unusual property of the human photopic b-wave was first described by Wali and Leguire,[11,12] and has been studied by many investigators.[13–17] Because a plot of the b-wave amplitude as a function of the stimulus intensity has an inverted U shape, this phenomenon has been named the "photopic hill." It has recently been reported that this phenomenon is flash dependent, and similar results are observed at different levels of light adaptation.[16]

The exact mechanism for the photopic hill has not been determined, although several hypothesis have been proposed: a summation of the negative a-wave and the positive b-waves,[11] an interaction of the depolarizing bipolar cells (DBCs) and hyperpolarizing bipolar cells (HBCs),[16,17] and a reduction of the OFF-response (d-wave) at higher stimulus intensities.[14]

The purpose of this study was to determine the mechanism underlying the photopic hill phenomenon. We asked two questions: first, whether the inner retinal neurons contribute to the photopic hill and, second, how the postreceptoral ON- and OFF-pathways contribute to the photopic hill. To address these questions, we recorded photopic flash ERG b-waves elicited by different stimulus intensities in monkeys. We used pharmacologic agents to isolate the activities from the different retinal cells and pathways.

MATERIALS AND METHODS

Subjects

Two rhesus (*Macaca mulatta*) and three cynomolgus (*M. fascicularis*) monkeys were studied. The animals were anesthetized with an intramuscular injection of ketamine hydrochloride (7 mg/kg, 5–10 mg/kg per hour maintenance dose) and xylazine (0.6 mg/kg). Respiration and heart rate were monitored, and hydration was maintained by slow, continuous subcutaneous infusion of lactated Ringer's solution. The cornea was anesthetized by topical 1% tetracaine, and the pupil was dilated with topical 0.5% tropicamide, 0.5% phenylephrine HCl, and 1% atropine. Experiments were conducted in accordance with NIH guidelines on animal use and with the ARVO Statement for the Use of Animals in Ophthalmic and Vision Research.

ERGs were also recorded from four normal human subjects (age range, 28–37 years). Informed consent was obtained from all subjects after a full explanation of the procedures. All studies were conducted in accordance with the principles embodied in the Declaration of Helsinki.

Visual Stimulation

Ganzfeld ERGs were elicited by xenon photostrobe flashes with a nominal flash duration at half height of 10 to 30 μs (color temperature, 5700° K). The Ganzfeld dome also housed the rod-suppressing background light of 40 cd/m^2. The maximum flash intensity measured in the dome was 2.30 log cd-s/m^2, which produced a maximum retinal intensity of 4.00 log photopic troland/s. The

From the Department of Ophthalmology, Nagoya University School of Medicine, Nagoya, Japan.

Supported by Grants-in-Aid 14770952 (MK), 13307048 (YM), and 14370557 (HT) from the Ministry of Education, Science, Sports and Culture, Japan.

Submitted for publication June 26, 2003; revised October 14, 2003; accepted October 31, 2003.

Disclosure: **S. Ueno**, None; **M. Kondo**, None; **Y. Niwa**, None; **H. Terasaki**, None; **Y. Miyake**, None

The publication costs of this article were defrayed in part by page charge payment. This article must therefore be marked "*advertisement*" in accordance with 18 U.S.C. §1734 solely to indicate this fact.

Corresponding author: Mineo Kondo, Department of Ophthalmology, Nagoya University School of Medicine, 65 Tsuruma-cho, Showa-ku, Nagoya 466-8550, Japan; kondomi@med.nagoya-u.ac.jp.

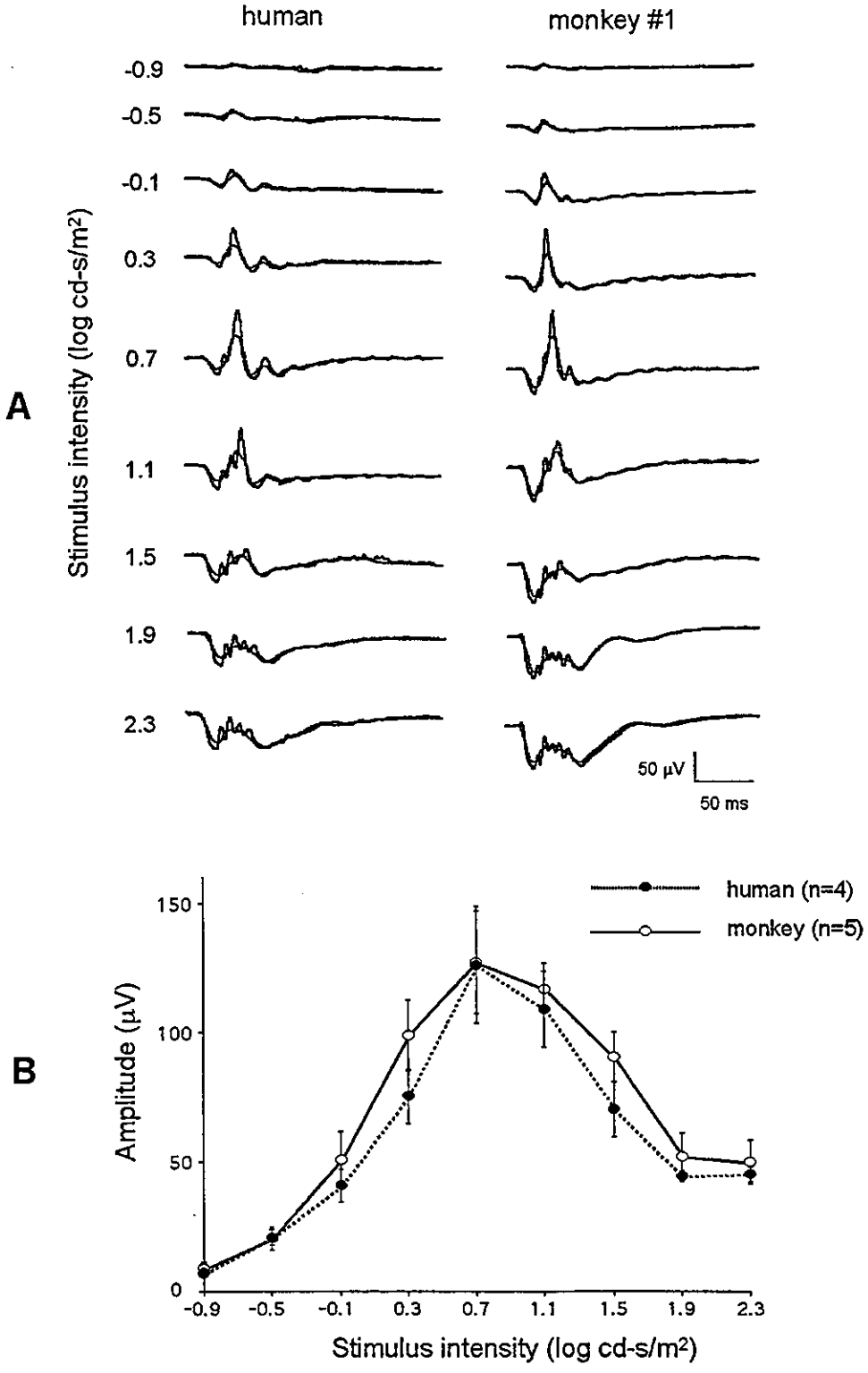

FIGURE 1. (A) Photopic flash ERGs elicited by different stimulus intensities recorded from a representative normal human subject and monkey 1. The waveforms after filtering the high-frequency OPs (100–300 Hz, *gray trace*) are superimposed on the actual ERG waveforms (*black trace*). (B) The intensity-response curves of the mean photopic b-wave amplitudes in four humans and five monkeys. Means ± SEM are plotted.

stimulus luminance was attenuated over a range of 3.2 log with neutral-density filters (Wratten; Eastman Kodak, Rochester, NY) in steps of 0.4 log units.

To monitor the drug effect on the monkey ERGs, 200-ms flashes were also recorded using a densely packed array of 102 green LEDs (525 nm peak wavelength; 50 nm at half amplitude), which was positioned on the top of the Ganzfeld dome and covered by a diffuser. The LEDs were controlled by a digital function generator (model WF1945; NF Corp., Tokyo, Japan). The stimulus intensity measured in the dome was 2.48 log cd/m^2, and the stimulus was presented on a white background luminance of 40 cd/m^2.

ERG Recording and Analysis

After an initial 10 minutes of light adaptation at 40 cd/m^2, ERGs were recorded with a Burian-Allen bipolar contact lens electrode (Hansen Ophthalmic Development Laboratories, Iowa City, IA). A ground electrode was attached to the ipsilateral ear. Responses were amplified

with a band-pass of 0.3 to 1000 Hz and digitized at 4.3 kHz. Contamination from line noise was reduced with a 60-Hz notch filter. To minimize the adaptational effect of high intensity stimuli, a small number of responses (three to six) were averaged and a long interstimulus interval of 15 to 240 seconds, depending on stimulus intensity, were used (Power Laboratory; AD Instruments, Castle Hill, New South Wales, Australia).

Drug Application

Drugs were injected into the vitreous with a 30-gauge needle inserted through the pars plana approximately 4 mm posterior to the limbus. Drugs (Sigma-Aldrich, St. Louis, MO) were dissolved in sterile saline and injected in amounts of 0.05 to 0.07 mL. Drugs and intravitreous concentrations were L-2 amino-4-phosphonobutyric acid (APB), 1 mM; *cis*-2,3 piperidine dicarboxylic acid (PDA) 5 mM; tetrodotoxin citrate (TTX), 4 μM; and *N*-methyl-D-aspartic acid (NMDA), 4 mM. Recordings were begun approximately 60 to 90 minutes after drug injections, and studies were completed within 5 hours. Although the drug effects are mostly reversible after a recovery period of several weeks, the results that are shown were recorded from the eyes not previously treated.

We were not able to separate the neural activities of DBCs and HBCs completely. We initially injected TTX+NMDA, APB, and PDA continuously to separate these components in a single experiment[10,18] but could not obtain reliable data because of unstable recording conditions due to the duration of the experiment.

Results

Intensity–Response Function of Photopic ERG b-Wave in Humans and Monkeys

The photopic ERGs elicited by different stimulus intensities and recorded from a representative human and monkey are shown in Figure 1A. The waveforms after filtering the high-frequency OPs (100–300 Hz, gray traces) are superimposed on the actual ERG waveforms (black traces). The means ± SE of the means (SEM) of the b-wave amplitude for four humans and five monkeys are plotted in Figure 1B.

The waveforms and intensity-response functions of the b-wave were quite similar in the humans and monkeys. As expected, the amplitude of the b-waves increased with increasing stimulus intensities, then reached a maximum at approximately 0.7 cd-s/m^2. Further increases in the stimulus intensity led to a rapid decline in the b-wave amplitude. These findings agree with previous studies in humans,[11–17] and the stimulus intensity that elicited the maximum b-wave amplitude was approximately the same as the value reported earlier.[11–17] The similarities in the photopic ERGs in humans and monkeys justified the use of monkeys to investigate the mechanism of the photopic hill seen in the human ERGs.

Effect of Blocking Inner Retinal Neural Activity by TTX and NMDA

First, we asked whether the inner retinal neurons are contributing to the photopic hill. To test this question, we applied TTX and NMDA, because TTX blocks voltage-gated sodium channels and prevents action potentials of ganglion cells and some kinds of amacrine cells.[19–21] NMDA suppresses synaptic transmission by its antagonistic action (depolarization) on the NMDA subclass of glutamate receptors located primarily on the third-order neurons.[22,23] It is thought that the intravitreous injection of TTX+NMDA can suppress most, if not all, electrical activities from inner retinal neurons.[10,18,24]

The photopic ERGs elicited by different stimulus intensities before and after the intravitreal injection of TTX+NMDA are shown in Figure 2 for one monkey (monkey 2). In the right column, the ERGs after TTX+NMDA (black traces) are superimposed on the control waveforms (gray traces). Both the amplitude and implicit times of the photopic ERG b-wave did not change significantly after TTX+NMDA to all stimulus intensities. The intensity-response curves of the photopic ERG b-wave before and after TTX+NMDA were also very similar, and both showed the photopic hill. These results indicated that the contribution from inner retinal neurons to the photopic hill is small.

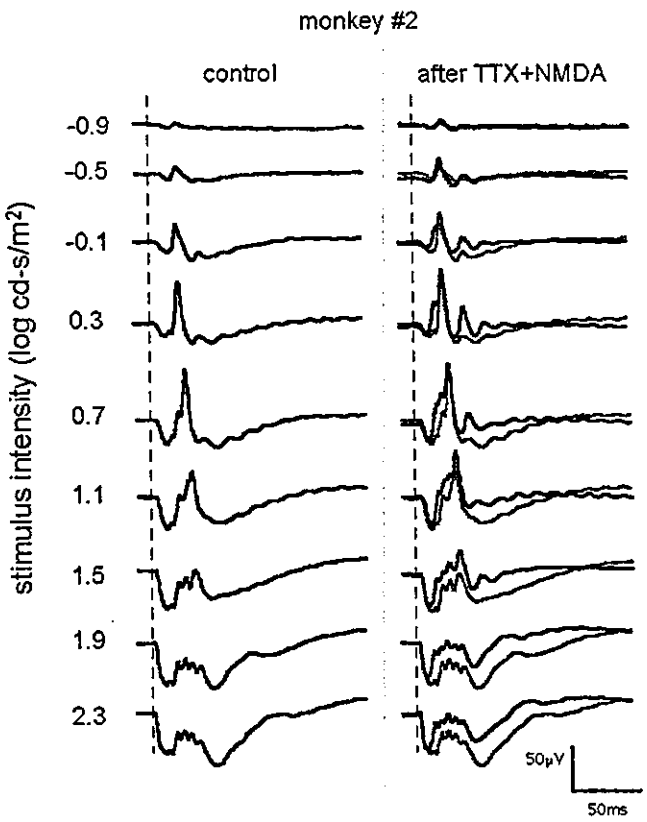

FIGURE 2. Photopic flash ERGs elicited from monkey 2 by different stimulus intensities before and after the injection of TTX+NMDA. ERGs after administration of drugs (*black trace*) are superimposed on the control ERGs (*gray trace*).

We also noted that the amplitude of the OPs was slightly reduced after injection of TTX+NMDA, and the late negative component (photopic negative response, PhNR) became smaller as reported by Viswanathan et al.[7] It was also noted that at low and intermediate stimulus intensities, another positive component after the b-wave, the i-wave, became prominent after TTX+NMDA.[7]

Effect of Blocking ON-Pathway by APB

Next we asked how the postreceptoral ON- and OFF-pathways contribute to the photopic hill. For this, we first injected APB[25] to block the activities of the postreceptoral ON-pathway and then PDA[26] to block the OFF-pathways. We then isolated the ON- and OFF-components by subtracting the postdrug ERGs from the predrug ERGs.

The photopic ERGs elicited by different stimulus intensities after APB in two monkeys (monkeys 3 and 4) are shown in Figure 3A. The waveforms after APB (black traces) are superimposed on the control waveforms (gray traces). Even after blocking the postsynaptic ON-pathway by APB, a sharp positive peak (d-wave[5,27]) remained at low and intermediate stimulus intensities (−0.9–0.7 log cd-s/m^2). However, the implicit

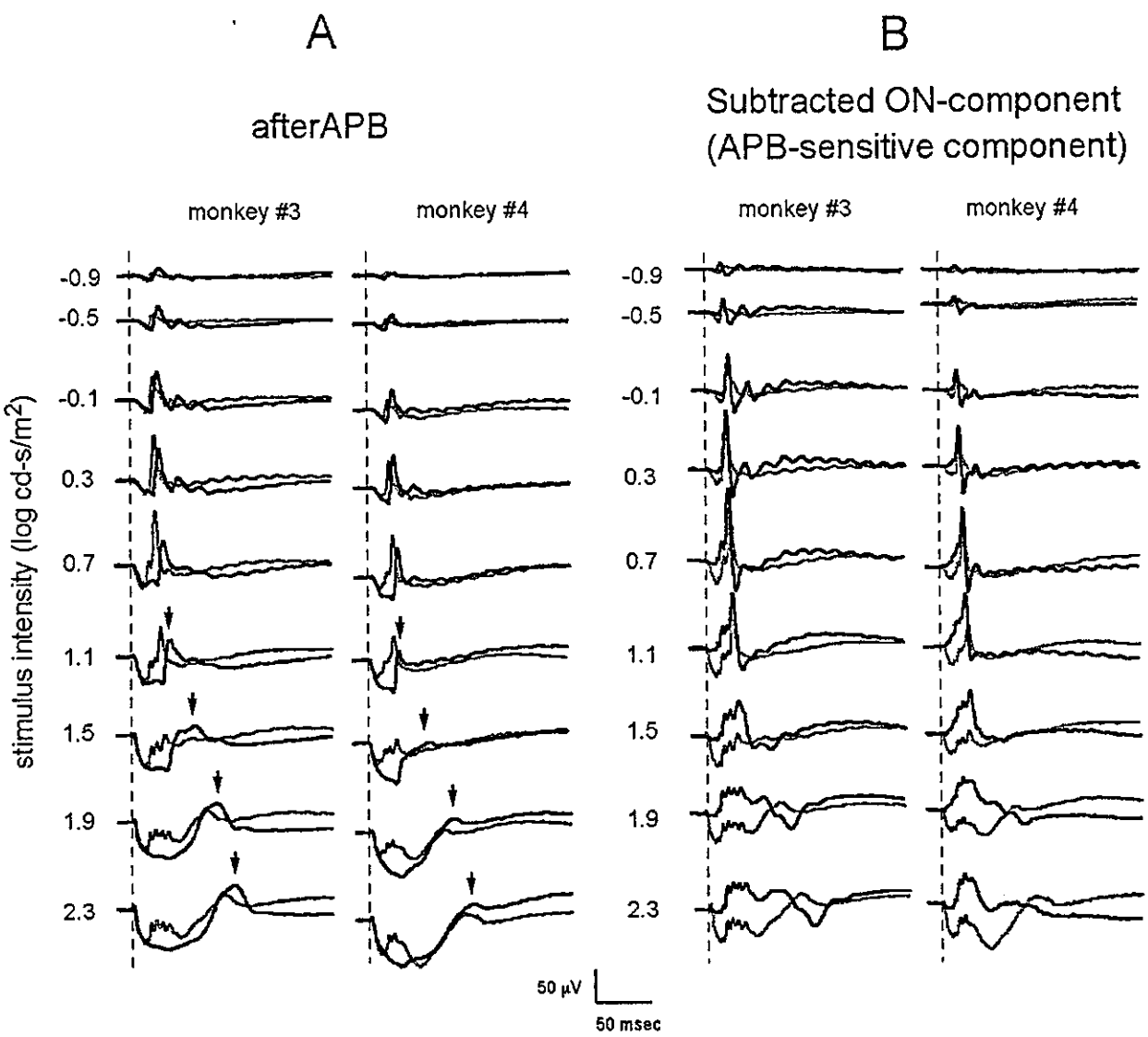

FIGURE 3. (A) Photopic flash ERGs elicited by different stimulus intensities before and after APB treatment in two animals (monkeys 3 and 4). ERGs after administration of APB (*black traces*) are superimposed on the control ERGs (*gray traces*). (B) Subtracted ON-components to different stimulus intensities. ON-components (APB-sensitive components) were obtained by subtracting the post-APB records from the control records. Results from two animals are shown (monkey 3 and 4).

time of this positive peak was 4 to 7 ms later than the implicit time of the control b-wave.

At higher stimulus intensities of 1.1 to 2.3 log cd-s/m^2, this positive component became less sharp, and its implicit time was increasingly prolonged (Fig. 3A, arrows). At higher stimulus intensities, the time of this positive peak moved far from that of control b-wave, and a deep, wide negative wave dominated the response.

The subtracted ON-components (APB-sensitive component) at the different stimulus intensities are shown in Figure 3B. The ON-component had a sharp positive peak at low and intermediate stimulus intensities (−0.9 - 0.7 log cd-s/m^2). With increasing intensities, the amplitude of this positive peak first increased but then decreased. The stimulus intensity which elicited maximal amplitudes of this positive peak was 0.7 log cd-s/m^2, which was the same stimulus intensity that elicited maximum b-wave amplitude in the control eyes.

At higher intensities, the amplitude of this positive wave became smaller, and the waveform became wider. These results strongly suggested that the amplitude reduction of the positive ON-component at higher stimulus intensities significantly contributed to the photopic hill.

Effect of Blocking the OFF-Pathway with PDA

The next step was to test whether the neural activity of the postsynaptic OFF-pathway contributes to the photopic hill. For this, we added PDA after APB in the same two eyes (monkeys 3 and 4). This also allowed us to determine whether the cone photoreceptors contributes to the photopic hill.

The photopic ERGs recorded after injection of APB+PDA are shown in Figure 4A. The intensity-response function of the isolated photoreceptor response is also plotted in the lower trace of Figure 4A. After APB+PDA, nearly all positive components were lost at all stimulus intensities. These results indicated that the cone photoreceptors do not contribute to the photopic hill directly. It was also noted that the contribution from the cone photoreceptors to the a-wave is minor at lower stimulus intensities.[6]

With increasing stimulus intensities, this negative photoreceptor component gradually became deeper and wider.

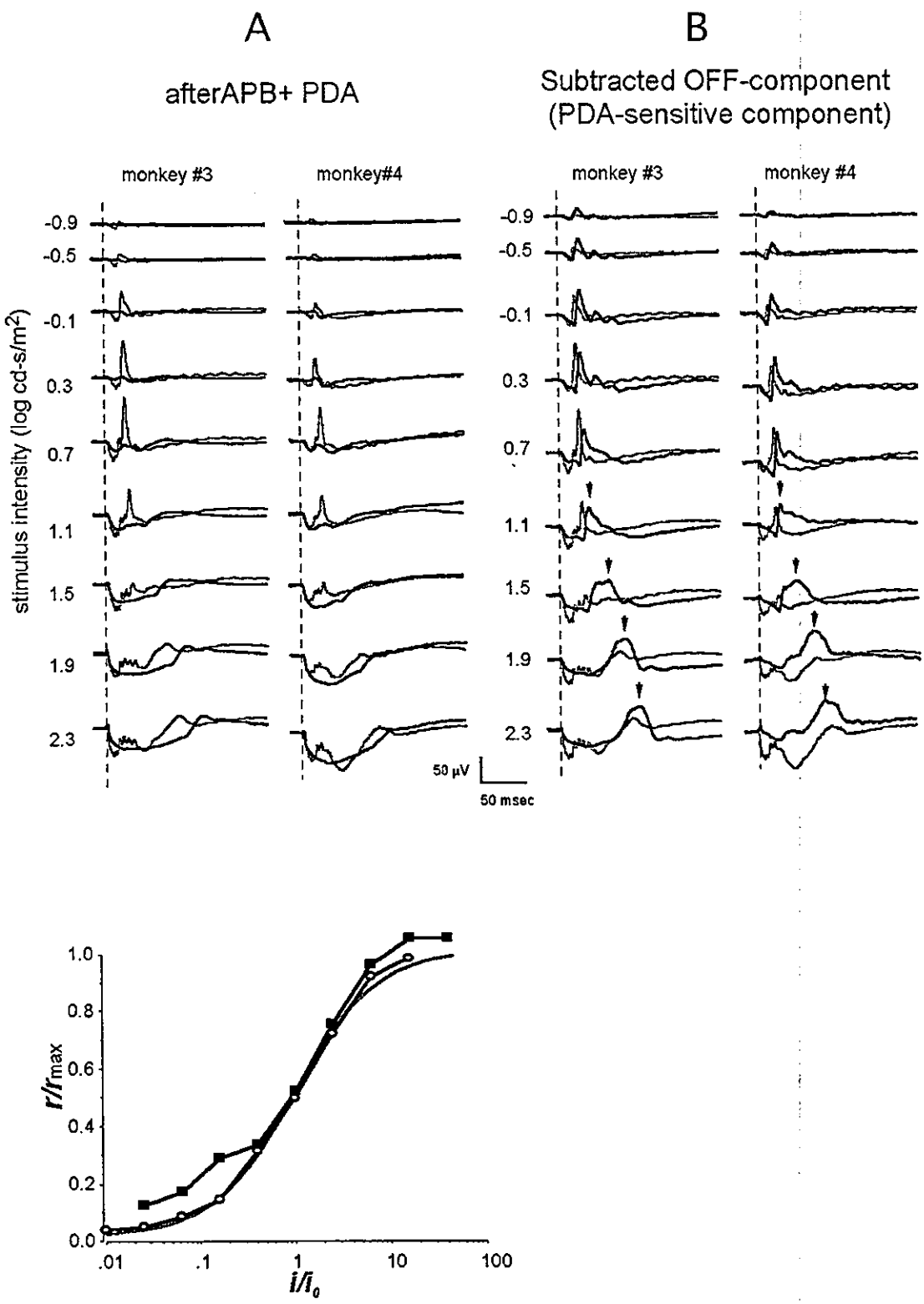

FIGURE 4. (A) *Top trace*: photopic flash ERGs elicited by different stimulus intensities before and after APB+PDA injection in the same two animals. ERGs after injection of APB+BDA (*black traces*) are superimposed on the control ERGs (*gray traces*). *Bottom trace*: response amplitude of two monkeys after APB+PDA is plotted as a function of flash strength on normalized axes. (○) Monkey 3; (■) monkey 4; r, response amplitude; r_{max} maximum response to saturating stimulus; i, flash stimulus intensity; i_0 the flash intensity elicited a peak response of one half r_{max}. *Gray line*: Michaelis function, $r/r_{max} = i/(i+i_0)$; (B) Subtracted OFF-components to different stimulus intensities. OFF-component (PDA-sensitive components) was obtained by subtracting the post-APB+PDA records from the post-APB records. Results from the same two animals are shown (monkey 3 and 4). Subtracted responses (*black traces*) are superimposed on the control ERGs (*gray traces*).

Past studies using whole-cell voltage and current recordings from macaque cone photoreceptors showed a similar delayed recovery of the receptor potential at stimulus intensities that saturate the negative receptor response.[28-30] This study of single photoreceptors also showed that the amplitude–intensity relation followed a Michaelis function, as our data after APB+PDA show (lower half of Fig. 4A).[29] However, the duration of the isolated a-wave in our study was not longer than the cone photoreceptor studies would predict.[28-30]

The amplitudes of this photoreceptor component were consistently smaller than those after APB alone. These findings also agreed with previous findings that in addition to the cone photoreceptors, other proximal retinal neurons (e.g., HBCs), contribute to the photopic ERG a-wave.[6]

The subtracted OFF-component (PDA-sensitive component) at the different stimulus intensities are shown in Figure 4B. As with the ON-component, the OFF-component had a sharp positive peak at low and middle stimulus intensities. Although the time of this positive peak was slightly later (4–7 msec) than that of the control b-wave, it is clear that this positive peak of the OFF-component contributed to the control b-wave at these stimulus intensities. The amplitude of this positive component became larger with increasing intensities at lower stimulus levels (−0.9–0.3 log cd-s/m^2), and then became slightly small and broader at higher intensities. In addition, the implicit time of this positive component was gradually prolonged with increasing intensities (arrowheads). At the highest stimulus intensity, a deep, wide negative wave dominated at the timing of the control ERG b-wave. These results indicate that the striking delay in the positive peak of the OFF-component at higher intensities contribute to the photopic hill.

Effect of PDA Alone

Finally, we wanted to see how the photopic flash ERG b-waves are altered after application of PDA alone to different stimulus intensities. PDA blocks not only the HBCs, but also other neural activity in the outer and inner plexiform layers.[26,31,32] This experiment is important because PDA removes the effect of the horizontal cells, and one can test the hypothesis that inhibitory feedback from the horizontal cells is the cause of the photopic hill.

The intensity response series of the photopic ERG after injection of PDA alone in two monkeys (monkeys 1 and 5) are shown in Figure 5. After application of PDA alone, the amplitude of the b-wave became larger with increasing intensities at lower and intermediate intensities, then reached a maximum at approximately 0.7 cd-s/m^2. At higher stimulus levels, the amplitude became small, and the waveform became wider. At maximum intensity, the amplitudes of the positive peak were 51% and 71% of those at 0.7 cd-s/m^2 in the two eyes. Although the photopic hill was smaller than average (45%, see Fig. 1), these results indicated that the photopic hill remained, even after the effects of the horizontal cells were suppressed. This suggests that inhibitory feedback is not the main mechanism for the photopic hill.

Discussion

Our results are summarized in Figure 6 based on data obtained from monkey 3. The waveforms of the three components—photoreceptoral, ON-, and OFF-components—are shown in different colors at three stimulus levels: low (−0.5 log cd-s/m^2), intermediate (0.3 log cd-s/m^2), and high (2.3 log cd-s/m^2) intensities.

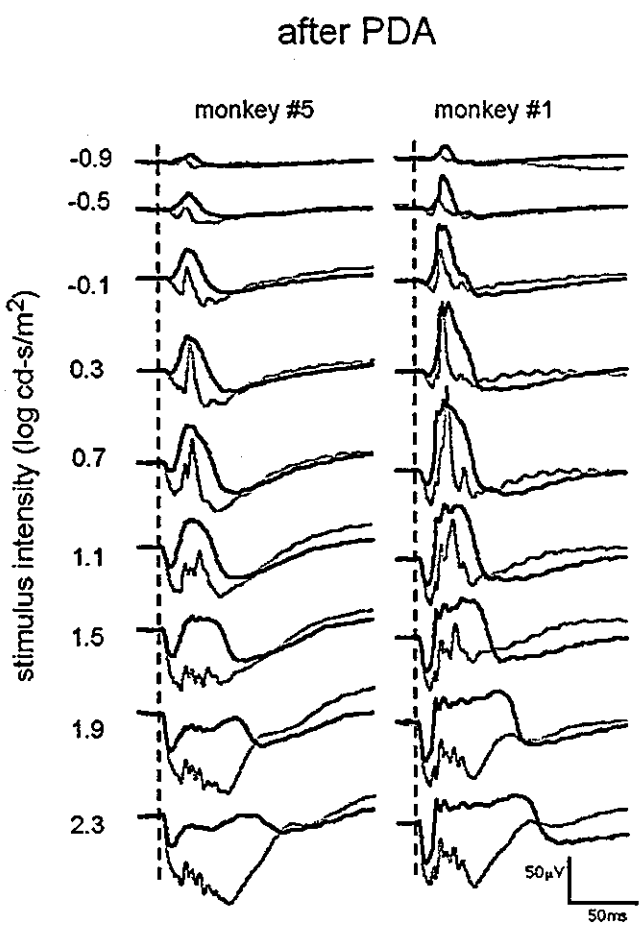

FIGURE 5. Photopic flash ERGs elicited by different stimulus intensities before and after PDA alone for two animals (monkeys 1 and 5). ERGs after PDA (*black traces*) are superimposed on the control ERGs (*gray traces*).

It has been proposed that the passive addition of negative and positive potentials of the photoreceptoral, ON-, and OFF-pathways may be involved in generating the photopic hill.[16,17] Our results partly agree with this proposal. As shown in the right column in Figure 6, the wide positive wave of the ON-component appeared to interfere with the wide negative OFF- and photoreceptoral components at higher stimulus levels. However, the magnitude of the contribution of this effect to the photopic hill was not as large when compared with two main factors, which will be described later. In addition, it is clear that this passive addition of negative and positive potentials for generating the b-wave exists even at low and intermediate intensities, because there was a timing lag between the two positive peaks (Fig. 6, left and middle columns).[5,10] Thus, although the passive additive effect of negative and positive potentials may also contribute to the generation of the photopic hill, its share is probably relatively small.

Our results demonstrated clearly that the photopic hill results mainly from the neural activity of the postreceptoral ON- and OFF-pathways. At low and intermediate stimulus intensities, the photopic b-wave is shaped by the overlapping of two positive peaks of the ON- and OFF-components, as expected from earlier studies.[5,10] At these stimulus intensities, the amplitudes of these two positive peaks increased with increasing stimulus intensities summing to result in the increase in the amplitude of the b-wave (Fig. 6, left and middle column). At higher stimulus intensities, however, the positive peak of the

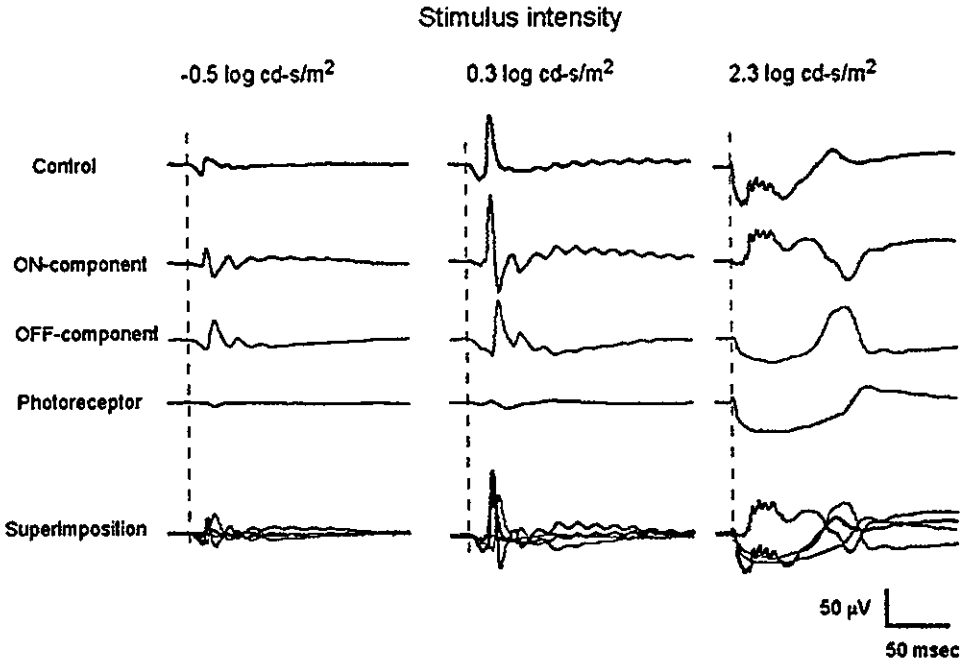

FIGURE 6. The photoreceptoral (*red*) and the postreceptoral ON- (*blue*) and OFF- (*green*) components of the photopic flash ERGs at three stimulus levels. Each component at low (−0.5 log cd-s/m^2), middle (0.3 log cd-s/m^2), and high (2.3 log cd-s/m^2) stimulus intensities from monkey 3 is shown.

ON-component became smaller and broader. In addition, the positive peak of the OFF-component was dramatically delayed with increasing intensity, and no longer contributed to the photopic b-wave (Fig. 6, right column). Thus, the resultant b-wave decreased.

From these results, we conclude that the photopic hill results mainly from two factors: the amplitude reduction of the ON-component at higher intensities and the delay in the positive peak of the OFF-component at higher intensities. Our results also indicate that the contribution from inner retinal neurons to the photopic hill is minor, because both the implicit times and amplitude of the photopic b-wave did not change much after TTX and NMDA at all stimulus intensities (Fig. 2). We also confirmed that the contribution of inhibitory feedback from the horizontal cells to the photopic hill is small, because the photopic hill, although somewhat reduced in amplitude in at least one animal, remained even with application of PDA alone (Fig. 5).

The positive component from the APB-sensitive component, presumably generated by DBCs, increased at low and middle intensities, and then became smaller and broader at higher stimulus intensities (Fig. 3B). Whether these results can predict the shape of the intensity-response function of the cone DBCs in monkeys is still uncertain, because there have been very few reports on the intensity-response function of the light-evoked potentials in the single cone DBCs in the mammalian retina. However, Berntson and Taylor[33] studied the light-evoked responses from bipolar cells in the mouse, and reported that the amplitude of the photovoltage of cone DBCs increased with increasing stimulus intensity and then reached a plateau at higher stimulus intensity. There was no notable amplitude reduction in the photovoltage of cone DBCs, even at the highest intensities in the mouse. The reason for the discrepancy between their results and ours may be explained by differences in experimental conditions and species. First, they used a long-duration stimuli (390 ms), whereas we used brief xenon flashes (<30 μs). It is known that the photopic hill is seen only when brief-flash stimuli are used. Second, they used mouse retina, whereas we used monkey retina. It has recently been reported that the photopic hill is less prominent in rodents (Joly S, et al. *IOVS* 2002;43:ARVO E-Abstract 1782). To address the question of whether our results can predict the electrical function of monkey cone DBCs, further studies on the intensity-response function on a single DBC in primate are needed.

The results obtained with PDA (Fig. 4) indicated that a portion of the photopic hill occurs because the positive HBC response becomes more delayed at higher flash levels, so that it adds less efficiently to the DBC (APB-sensitive) component. This situation can be mimicked at lower flash levels by extending the duration of the stimulus so that the positive OFF-response is shifted in time. Actually, past studies have reported that the amplitude of the b-wave decreases with increasing flash duration (for example, Ref. 14).

The exact mechanism for the delay in the positive PDA-sensitive component at higher stimulus intensity is also unclear, because there have been no reports on the intensity-response function of single cone HBCs in monkeys. One plausible explanation is that this stimulus-dependent delay could reflect the longer time course needed for cone photoreceptors to recover after strong flashes. The isolated cone photoreceptor responses shown in Figure 4A and data from the single-cell recordings from macaque cone photoreceptors[28-30] are consistent with this idea.

In conclusion, the photopic hill in the primate ERG results mainly from two factors: the amplitude reduction of the ON-component at higher intensities and the delay in the positive peak of the OFF-component at higher intensities. To determine the exact cellular mechanism underlying this phenomenon, further studies on the intensity-response function in primate cone bipolar cells are needed.

Acknowledgments

The authors thank Masao Yoshikawa, Eiichiro Nagasaka, and Hidetaka Kudo of Mayo Co. (Nagoya, Japan) and Hiroyuki Sakai of Santen Co. (Osaka, Japan) for technical help.

References

1. Brown KT, Watanabe K. Isolation and identification of the receptor potential from the pure cone fovea of the monkey retina. *Nature (Lond).* 1962;193:958-960.

2. Knapp AG, Schiller PH. The contribution of on-bipolar cells to the electroretinogram of rabbits and monkeys: a study using 2-amino-4-phosphonobutyrate (APB). *Vision Res.* 1984;24:1841-1846.
3. Heynen H, Wachtmeister L, von Norren D. Origin of the oscillatory potentials in primate retina. *Vision Res.* 1985;10:1365-1373.
4. Evers HU, Gouras P. Three cone mechanisms in the primate electroretinogram: two with, one without off-center bipolar responses. *Vision Res.* 1986;26:245-254.
5. Sieving PA, Murayama K, Naarendorp F. Push-pull model of the primate photopic electroretinogram: a role for hyperpolarizing neurons in shaping the b-wave. *Vis Neurosci.* 1994;11:519-532.
6. Bush RA, Sieving PA. A proximal retinal component in the primate photopic ERG a-wave. *Invest Ophthalmol Vis Sci.* 1994;35:635-645.
7. Viswanathan S, Frishman LJ, Robson JG, Harwerth RS, Smith EL III. The photopic negative response of the macaque electroretinogram: reduction by experimental glaucoma. *Invest Ophthalmol Vis Sci.* 1999;40:1124-1136.
8. Viswanathan S, Frishman LJ, Robson JG. The uniform field and pattern ERG in macaques with experimental glaucoma: removal of spiking activity. *Invest Ophthalmol Vis Sci.* 2000;41:2797-2810.
9. Robson JG, Saszik SM, Ahmed J, Frishman LJ. Rod and cone contributions to the a-wave of the electroretinogram of the dark-adapted macaque. *J Physiol.* 2003;547:509-530.
10. Rangaswamy NV, Hood DC, Frishman LJ. Regional variations in the local contributions to the primate photopic flash ERG revealed using the slow-sequence mfERG. *Invest Ophthalmol Vis Sci.* 2003; 44:3233-3247.
11. Wali N, Leguire LE. The photopic hill: a new phenomenon of the light adapted electroretinogram. *Doc Ophthalmol.* 1992;80:335-342.
12. Wali N, Leguire LE. Fundus pigmentation and the electroretinographic luminance-response function. *Doc Ophthalmol.* 1993;84: 61-69.
13. Peachey NS, Alexander KR, Derlacki DJ, Fishman GA. Light adaptation and the luminance-response function of the cone electroretinogram. *Doc Ophthalmol.* 1992;79:363-369.
14. Kondo M, Piao CH, Tanikawa A, Horiguchi M, Terasaki H, Miyake Y. Amplitude decrease of photopic ERG b-wave at higher stimulus intensities in humans. *Jpn J Ophthalmol.* 2000;44:20-28.
15. Lachapell P, Rufiange M, Dembinska O. A physiological basis for definition of the ISCEV ERG standard flash (SF) based on the photopic hill. *Doc Ophthalmol.* 2001;102:157-162.
16. Rufiange M, Rousseau S, Dembinska O, Lachapelle P. Cone-dominated ERG luminance-response function: the photopic hill revisited. *Doc Ophthalmol.* 2002;104:231-248.
17. Rufiange M, Dassa J, Dembinska O, et al. The photopic ERG luminance-response function (photopic hill): method of analysis and clinical application. *Vision Res.* 2003;43:1405-1412.
18. Robson JG, Frishman LJ. Response linearity and kinetics of the cat retina: the bipolar cell component of the dark-adapted electroretinogram. *Vis Neurosci.* 1995;12:837-850.
19. Narahashi T, Moore JW, Scott WR. Tetrodotoxin blockage of sodium conductance increase in lobster giant axons. *J Gen Physiol.* 1964;47:965-974.
20. Narahashi T. Chemicals as tools in the study of excitable membranes. *Physiol Rev.* 1974;54:813-889.
21. Bloomfield SA. Effect of spike blockade on the receptive-field size of amacrine and ganglion cells in the rabbit retina. *J Neurophysiol.* 1996;75:1878-1893.
22. Slaughter MM, Miller RF. The role of excitatory amino acid transmitters in the mudpuppy retina: an analysis with kainic acid and N-methyl aspartate. *J Neurosci.* 1983;3:1701-1711.
23. Massey SC. Cell types using glutamate as a neurotransmitter in the vertebrate retina. *Prog Retin Res.* 1990;10:399-426.
24. Hood DC, Frishman LJ, Saszik S, Viswanathan S. Retinal origins of the primate multifocal ERG: implications for the human response. *Invest Ophthalmol Vis Sci.* 2002;43:1673-1685.
25. Slaughter MM, Miller RF. 2-amino-4-phosphonobutyric acid: a new tool for retina research. *Science.* 1981;211:182-185.
26. Slaughter MM, Miller RF. An excitatory amino acid antagonist blocks cone input to sign-conserving second-order retinal neurons. *Science.* 1983;219:1230-1232.
27. Frishman LJ, Karwoski CJ. b-wave. In: Heckenlively JR, Arden GB, eds. *Handbook of Clinical Electrophysiology of Vision Testing.* St. Louis: Mosby Year Book; 1991:112-114.
28. Schnapf JL, Nunn BJ, Meister M, Baylor DA. Visual transduction in cones of the monkey *Macaca fascicularis. J Physiol (Lond).* 1990; 427:681-713.
29. Schneeweis DM, Schnapf JL. Photovoltage of rods and cones in the macaque retina. *Science.* 1995;268:1053-1056.
30. Schneeweis DM, Schnapf JL. The photovoltage of macaque cone photoreceptors: adaptation, noise, and kinetics. *J Neurosci.* 1999; 19:1203-1216.
31. Slaughter MM, Miller RF. Bipolar cells in the mudpuppy retina use an excitatory amino acid neurotransmitter. *Nature.* 1983;303:537-538.
32. Massey SC, Miller RF. Glutamate receptors of ganglion cells in the rabbit retina: evidence for glutamate as a bipolar cell transmitter. *J Physiol.* 1988;405:635-655.
33. Berntson A, Taylor WR. Response characteristics and receptive field widths of on-bipolar cells in the mouse retina. *J Physiol.* 2000;524:879-889.

Vitrectomy and Internal Limiting Membrane Peeling for Myopic Foveoschisis

YASUSHI IKUNO, MD, KAORI SAYANAGI, MD, MASAHITO OHJI, MD, MOTOHIRO KAMEI, MD, FUMI GOMI, MD, SEIYO HARINO, MD, TAKASHI FUJIKADO, MD, AND YASUO TANO, MD

• PURPOSE: Myopic foveoschisis is common in high myopia. We report results of a pilot study of vitrectomy for patients with myopic foveoschisis.
• DESIGN: Interventional case series.
• METHODS: In an institutional setting five patients with high myopia (six eyes), and who had progressive visual impairment presumably due to myopic foveoschisis were studied. No eyes had a macular hole preoperatively based on optical coherence tomography (OCT). We performed vitrectomy including vitreous cortex removal, internal limiting membrane (ILM) peeling, and gas tamponade. Patients were followed for at least 6 months. Best-corrected visual acuity (BCVA), OCT. Scanning laser ophthalmoscope (SLO) microperimetry was examined in three eyes.
• RESULTS: The foveal detachment resolved completely in five eyes and partially in one eye. No serious complications developed including macular hole formation or retinal detachment; BCVA improved more than two lines in all eyes (100%) 6 months postoperatively ($P < .01$); SLO microperimetry showed smaller scotoma compared with preoperatively and stabilized fixation.
• CONCLUSIONS: Vitrectomy with vitreous cortex removal, ILM peeling, and gas tamponade could be useful to treat myopic foveoschisis in highly myopic eyes. Because the natural course of the disease is not well-understood, further study should establish indications for this surgery. (Am J Ophthalmol 2004;137:719–724. © 2004 by Elsevier Inc. All rights reserved.)

MYOPIC FOVEOSCHISIS WITHOUT MACULAR HOLES has been observed in highly myopic eyes[1] and reported to occur in approximately 9% of patients with posterior staphyloma.[2] The pathogenesis is unknown; however, myopic foveoschisis is believed to be caused by vitreous traction[1,3–5] before macular hole formation.

Although the benefit of vitrectomy is uncertain for patients with myopic foveoschisis, some small pilot studies presented cases with visual improvement after vitrectomy.[6–8] Ishikawa and associates[6] performed vitrectomy with internal limiting membrane (ILM) peeling and gas tamponade in 15 eyes with myopic foveoschisis, and in 14 eyes the retina reattached after surgery. Those authors also reported that seven of 15 eyes (46.7%) achieved visual improvement greater than 0.3 logarithm of the minimal angle of resolution (logMAR). Kobayashi and associates[7] reported that they performed vitrectomy in nine eyes with myopic foveoschisis, and that in eight eyes (89%) retinal reattachment and visual improvement occurred; however, a macular hole developed in one eye.

We report the results of a study of vitrectomy including vitreous cortex removal using triamcinolone acetate, ILM peeling with indocyanine green (ICG) staining, and gas tamponade in six eyes of five patients with myopic foveoschisis who presented with progressive visual impairment.

METHODS

• PATIENTS: Five consecutive patients (six eyes) (one man, four women) who underwent vitrectomy for myopic foveoschisis were included in the study. Inclusion criteria were progressive visual loss presumably due to foveoschisis associated with high myopia, absence of retinal tears, and absence of a macular hole observed by optical coherence tomography (OCT). Patients underwent examinations that included best-corrected visual acuity (BCVA) measurement and OCT before and after surgery. In three eyes, scanning laser ophthalmoscope (SLO) microperimetry was also performed after we obtained informed consent from each patient. The follow-up period was at least 6 months.

Biosketches and/or additional material at www.ajo.com
Accepted for publication Oct 5, 2003.
From the Department of Ophthalmology, Osaka University Medical School, Suita, Japan.
Inquiries to Yasushi Ikuno, MD, Department of Ophthalmology, Rm. E7, Osaka University Medical School, 2-2 Yamadaoka, Suita 565-0871 Japan; fax: (+81) 6-6879-3458; e-mail: ikuno@ophthal.med.osaka-u.ac.jp

0002-9394/04/$30.00
doi:10.1016/j.ajo.2003.10.019

TABLE 1. Appearance and Visual Outcome of the Patients

No.	Gender	Age	R/L	Axial Length	Refractive Error	Duration of Symptoms (Months)	Preoperative Lens Status	Preoperative BCVA	Postoperative BCVA (6M)	Best BCVA	F/U (Months)
1	F	63	R	29.9	−20	6	Phakic	0.08 (20/250)	0.3 (20/60)	0.3 (20/60)	24
2	F	63	R	28.7	−11.25	2	Phakic	0.15 (20/120)	0.3 (20/60)	0.3 (20/60)	20
2	F	63	L	27.9	−13.75	96	Phakic	0.04 (20/500)	0.07 (20/300)	0.08 (20/250)	10
3	F	51	R	29.8	−12.5	3	Phakic	0.15 (20/120)	0.8 (20/25)	0.9 (20/25)	18
4	F	64	R	29.4	−14	2	Phakic	0.07 (20/300)	0.4 (20/50)	0.4 (20/50)	6
5	M	53	R	29.4	−15	3	Phakic	0.03 (20/600)	0.15 (20/120)	0.15 (20/120)	6

The approximate value on the Snellen visual acuity chart is indicated in parenthesis.
BCVA = best-corrected visual acuity; F = female; F/U = follow-up; L = left; M = male; R = right.

• SURGICAL PROCEDURE: All surgeries were performed by one author (Y.I.). To avoid cataract progression, phacoemulsification with simultaneous intraocular lens implantation was performed in all eyes followed by a conventional three-port vitrectomy. First, a core vitrectomy was performed, and the vitreous cortex, which was typically observed as a thin membrane, was removed completely from the surface of the posterior retina using a diamond-dusted membrane scraper[9,10] after visualization with triamcinolone acetate.[11] The ILM of 2 to 3 disk diameters was peeled with ICG staining (5 mg/ml) and asymmetric forceps. Finally, the vitreous cavity was replaced with air and gas tamponade using 16% perfluoropropane. Patients were instructed to maintain a prone position postoperatively for at least 2 weeks.

• SLO MICROPERIMETRY: Retinal function was assessed with SLO microperimetry in three eyes as described previously.[12,13] Briefly, we tried to detect a scotoma and the fixation point on the posterior retina by stimulating the retinal loci using a laser beam spot (diameter, 27.5 m; intensity, 0 dB; duration, 0.1 second) focused on the retina.

• OCT EXAMINATION: Optical coherence tomography was performed preoperatively and postoperatively using commercially available OCT equipment (Humphrey Instruments Inc., San Leandro, California, USA). The examination was performed using the default setting of the crosshair mode, which scans 5.65 mm vertically and horizontally on the retina. The height of the foveal detachment, defined as the distance between the inner surface of the retinal pigment epithelium and the outer surface of the neural retina at the fovea, was measured on the vertical scan image using the retinal thickness mode of the OCT application.

• STATISTICAL ANALYSIS: To evaluate the effect of surgery, the height of the foveal detachment preoperatively and postoperatively and the preoperative and postoperative BCVA were analyzed using Sigma Stat (SPSS, Inc, Chicago, Illinois, USA). Best-corrected visual acuity was converted to logMAR for the analysis. The paired t test was used, and $P < .05$ was considered to be significant.

RESULTS

THE PREOPERATIVE PATIENT DEMOGRAPHIC DATA ARE shown in Table 1. All eyes were phakic before surgery. The patient ages at the time of surgery ranged from 51 to 64 years (59.5 ± 5.9 years, mean ± standard deviation [SD]). The refractive errors ranged from −11.25 to −20.0 diopters (D) (−14.4 ± 3.0 D, mean ± SD). The axial lengths ranged from 27.9 to 29.9 mm (29.2 ± 0.8 mm, mean ± SD). The duration of symptoms ranged from 2 to 96 months (18.6 ± 37.9 months, mean ± SD). The follow-up period ranged from 6 to 24 months (14.0 ± 7.7 months, mean ± SD). Vision improved more than two lines in all eyes (100%) 6 months after surgery ($P < .01$). No serious intraoperative or postoperative complications including macular hole and/or peripheral retinal break formation, retinal detachment, or intraocular hemorrhage occurred.

The foveal changes in the OCT image before and 6 months after surgery are shown in Figure 1. Of the six study eyes, the foveal detachment completely resolved in five eyes (83%). The foveal detachment decreased but remained unresolved in one eye 6 months after surgery. The time course of the decrease in the height of the foveal detachment is shown in Figure 2. The height of the retinal detachment decreased significantly at 3 and 6 months after surgery ($P < .01$ for both comparisons).